A New Space Vector Modulation Pulse Width Modulation Technique for an Optimal Total Harmonic Distortion of a Three-Phase Voltage Source Inverter Power System

Hichem Benkadi, Tarek Ghennam, Khoudir Marouani, Nassim Rizoug, Mohamed Benbouzid, Bruno Francois

International Journal on Energy Conversion (IRECON), July 2023, 11(4), pp. 109–121, DOI:10.15866/irecon.v11i4.24157

A New Space Vector Modulation Pulse Width Modulation Technique for an Optimal Total Harmonic Distortion of a Three-Phase Voltage Source Inverter Power System

Hichem Benkadi[(1*)], Tarek Ghennam[(1)], Khoudir Marouani[(1,2)],Nassim Rizoug[(3)], Mohamed Benbouzid[(4)], Bruno Francois[(5)]

[(1)]Ecole Militaire Polytechnique, Bordj el Bahri16046, Algiers, Algeria
[(2)]University of Mouloud Mammeri,Tizi-Ouzou Algeria
[(3)]ESTACA LAB 53061, Montigny-le-Bretonneux, France
[(4)] University of Brest, UMR CNRS 60 IRDL, 29238 Brest, France
[(5)]University of Lille, Arts et Metiers Institute of Technology, Centrale Lille, Junia, ULR 2697 - L2EP, F-59000 Lille, France
Address correspondence to Hichem Benkadi, Ecole Militaire Polytechnique, Bordj el Bahri 16046, Algiers, Algeria. E-mail: benkadih@gmail.com

Abstract – *The voltage and current outputs of a power electronic converter contain high harmonic, especially when the required power operation point is less than the nominal one. The present paper proposes a new space vector modulation scheme to improve this harmonic content for the overall power range. This technique is based on an optimized distribution of the zero vectors during the sampling time. Firstly, a vector spatial approach of the voltage flux harmonic is analytically synthesized. Hence, the obtained flux harmonic trajectories are optimized somehow to minimize the distance between the gravity center of this trajectory and its origin, which gives the exact du- ration of the zero vectors. The obtained simulation and experimental results show an improved harmonic content of the output converter even for low modulation index and an enhanced converter current waveform. The results confirm the superiority of the proposed strategy compared to the previously developed.*

Keywords*: Source Inverter Inverter(VSI); Conventional Space Vector Modulation Pulse Width Modulation (CSVPWM); Random Zero Vector Distribution Space Vector Pulse Width Modulation (RZVDSVPWM); Modulation index (m); Total Harmonic Distortion (THD).*

List of Symbols

CSVPWM	Conventional Space Vector Pulse Width Modulation
DC	Direct Current
f_e	Reference frequency
f_s	Switching frequency
L	Inductor
m	Modulation index
R	Resistor
R-ZVD-SVPWM	Random Zero Vector Distribution Space Vector Pulse Width Modulation
SVPWM	Space Vector Pulse Width Modulation
THD	Total Harmonic Distortion
T_S	Application time
T_s	Sampling period
V_{dc}	DC-bus volage
V_k	Inverter output voltage vector of the k'th state
V_{ref}	Voltage Reference
VSI	Voltage Source Inverter
ZVD	Zero Vector Distribution
θ	Vector reference phase
φ_h	Harmonic flux

I. Introduction

Nowadays, Voltage Source Inverters (VSIs) are highly involved in most industrial electrical systems. In fact, these applications can be classified into two categories: power generation systems[1] and power drive systems[2]. The first category concerns all electrical energy conversion systems such as: wind energy systems, solar energy systems[3], conventional generation systems[4], uninterruptible power systems[5], active filters[6]…etc. These conversion systems require an enhanced energy quality output[7] for all the power ranges as well as a good efficiency[8].The second category includes all power drive systems, which are basically used for controlling the speed[9], torque[10] of an electric motor such as in electrical vehicles[11], aerospace applications[12], naval

Manuscript received January 2013, revised February 2013

propulsion[13] …etc. These power drive systems need a low torque ripple [14], low humming noises[15] and low electromagnetic interferences[12]. To achieve all these requirements of electrical systems, the VSI output should have a low harmonic content otherwise a low Total Harmonic Distortion (THD) that leads to an increased system efficiency[4].

These electrical systems have generally good performances (good efficiency) when they are controlled around their nominal power. However, in some cases when the required power is less than the nominal one, the system performances are reduced due to the increase of the VSI output harmonic distortion[16]. This phenomenon is the result of the VSI low modulation index (m) due to the decrease of the VSI output voltage reference compared to the total DC link voltage. In order to solve this problem and to upgrade the system performances, many ways can be distinguished. As example, the multilevel VSI is considered among the useful solution to overcome the mentioned problem[17], but this solution adds more switches and then more complexity and space constraints[18]. Another solution is to dynamically adapt the DC link voltage around the VSI output voltage reference in order to keep a high modulation index [19]. This solution requires another device to regulate the DC bus, which makes this structure more bulky and complex[20]. One more alternative is to develop a dedicated Space Vector Pulse Width Modulation (SVPWM) to deal with the previously mentioned problems and in this context, several research activities have been proposed [15].

By using a Conventional SVPWM (CSVPWM), rather than a triangular carrier-based modulation, the harmonic content is decreased and hence the maximum peak value of the output voltage is increased by 15%[21]. Nevertheless, it suffers from a high harmonic content when the modulation index is low. Recently, several research works have focused on random modulations[22], especially Random Zero Vector Distribution SVPWM(R-ZVD-SVPWM) for spreading the harmonic spectrum along the frequency range [23], but high harmonics still exist for low modulation index. The author in [22] proposes a method that combines the hysteresis selection of the two zero vectors with the random distribution. Thus, the zero vector V_7 is selected when m> 0.8 and as V_0 when m<0.8. The upgraded technique results confirm the correlation between the harmonic content and the ZVD but this technique is still suffering from a low modulation index. Then, it is not based on an exact mathematical development, which enables an optimal distribution of zero vector voltage.

*In this paper, a new SVPWM, for the VSI supplying a three-phase load (*Fig *1), is proposed to reduce the harmonic content in an optimal manner for the entire index modulation range. This strategy is based on an optimal ZVD, which is determined by using a vector spatial approach of the voltage flux harmonic. For this reason, an analytical development of harmonic flux has been established to minimize the gravity center of the drawn flux harmonic trajectories and their origin. Therefore, mathematical formulas of the ZVD have been developed to express the exact duration of the zero vectors during the sampling time. Simulation work has been performed by using Simulink/MATLAB. An experimental test bench has been built and the proposed technique has been implemented on a Dspace 1104 board. Simulation and experimental results showed performances of the proposed technique compared to the CSVPWM and R-ZVD-SVPWM.*

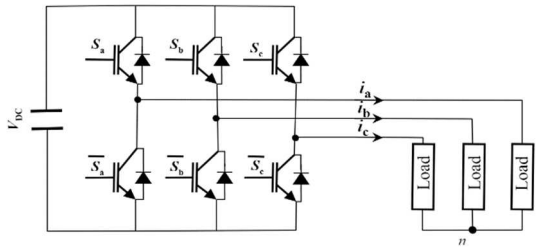

Fig 1. Three-phase VSI power system.

II. System Descriptions of SVPWM Switching Strategies

II.1. Presentation and fundamentals

A three-phase VSI generates eight switching states depending on (S_a, S_b, S_c) in FIG 1. The switching states present six active voltage vectors (V_1, V_2 V_3, V_4, V_5,and V_6) and two zero voltage vectors V_Z (V_0(000) and V_7(111)) in a complex plane (Fig 2). Therefore, SVPWM control strategy is based firstly on the representation of the required three-phase VSI output voltages in the complex plane that is divided into six (06) sectors. Then, depending on its location in one of these six sectors (Fig 2), two adjacent voltage vectors and zero voltage vectors will be employed to reproduce it.

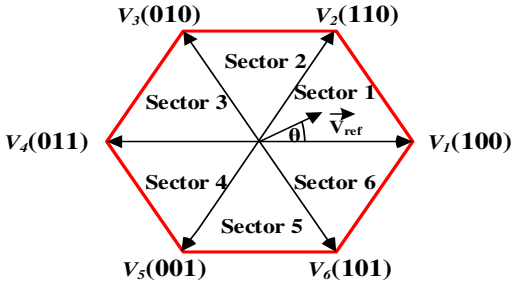

Fig 2. Space-vector diagram for the SVPWM.

The reference vector V_{ref} in sector one (Fig 2) can be expressed during the sampling time T_s by the following equations.

$$V_{ref} = \frac{T_1}{T_s}V_1 + \frac{T_2}{T_s}V_2 + \frac{T_z}{T_s}V_z \quad (1)$$

T_1, T_2, T_Z are respectively the duration of applied vectors V_1, V_2 and V_Z. The durations T_1, T_2, and T_Z can be given as follows:

$$T_1 = \frac{2\sqrt{3}}{\pi} m \sin(\frac{\pi}{3} - 2\pi f_e t) T_s \quad (2)$$

$$T_2 = \frac{2\sqrt{3}}{\pi} m \sin(2\pi f_e t) T_s \quad (3)$$

$$T_z = T_0 + T_7 = T_s - T_1 - T_2 \quad (4)$$

Where f_e is the reference frequency m is the modulation index, which is linked to the magnitude of the voltage reference V_{ref} and the DC link voltage V_{dc} by the following equation:

$$m = \frac{\pi V_{ref}}{2V_{dc}} \quad (5)$$

To simplify the mathematical expressions, the previous durations can be formulated in terms of the duty cycles, which are defined as the ratio between the application time and the sampling period (d_S=T_S/T_s). Therefore, the duty cycles of the adjacent vectors (d_i and d_{i+1}) and zero vectors d_z (d_0 and d_7) of any sector i can be given by:

$$d_S = \frac{2\sqrt{3}}{\pi} m \sin(S\frac{\pi}{3} - 2\pi f_e t) \quad (6)$$

$$d_{S+1} = \frac{2\sqrt{3}}{\pi} m \sin(2\pi f_e t - (S-1)\frac{\pi}{3}) \quad (7)$$

$$d_z = d_0 + d_7 = 1 - d_S - d_{S+1} \quad (8)$$

From the energetic point of view, the zero voltage vectors do not contribute to generate active power. In other words, the ZVD does not alter the fundamental of the VSI output voltage and current, but it affects their harmonic contents. Many research works have been carried out to improve the harmonic content of the CSVPWM, where an equally ZVD is applied, by using R-ZVD-SVPWM[24]. The duty cycles of the two zero vectors in CSVPWM are the same as in equation (9), while for random ZVD-SVPWM their duration changes randomly as is reported in equation (10)[23]. Fig 3. (a) and (b) show respectively the pulse patterns of the CSVPWM and random ZVD-SVPWM pulses.

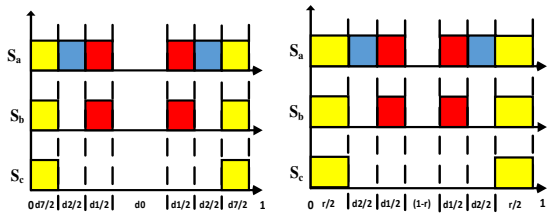

(a) (b)

Fig 3. SVPWM pulse patterns in sector 1. (a) CSVPWM. (b) R-ZVD-SVPWM.

$$\frac{1}{2} d_z = d_0 = d_7 \quad (9)$$

$$\begin{cases} d_7 = r \\ d_0 = 1 - r \end{cases} \quad (10)$$

r is a random number, that varies between 0 and 1.

The proposed technique employs an optimal ZVD to reduce the harmonic content of the VSI outputs by using a vector spatial approach of the voltage flux harmonic.

II.2. Concept of harmonic flux

The concept of harmonic flux is a mathematical method, that permits to evaluate the total harmonic generated by the modulation technique. The advantage of the harmonic flux is that no load information is required, and the switching frequency response of an inverter can be accurately characterized[25].The harmonic flux is based on the vector spatial approach, which is considered as one of the simplest and most insightful approaches for the analytical characterization of the switching frequency harmonics of a VSI. For the well explanation of this approach, the first sector of the inverter hexagon is taken as an instance (Fig 4). The vector diagram illustrates how the harmonic voltage vectors V_{1h}, V_{2h},and V_{0h} are generated in each carrier cycle. In fact, the voltage vector reference must be produced by the two active vectors ($V_1$and V_2) and the zero vectors (V_0 and V_7) by using equation (1). However, from the vector representation point of view, when the adjacent vectors are applied during the sampling time the harmonic voltage vectors V_{1h}, V_{2h}, and V_{0h} have to be generated to balance the reference vector (Fig 4):

$$\begin{cases} \vec{V}_{1h} = \vec{V}_1 - \vec{V}_{ref} \ when \quad \vec{V}_1 \ is \quad applied \\ \vec{V}_{2h} = \vec{V}_2 - \vec{V}_{ref} \ when \quad \vec{V}_2 \ is \quad applied \\ \vec{V}_{0h} = \vec{V}_0 - \vec{V}_{ref} \ when \quad \vec{V}_0 \ is \quad applied \end{cases} \quad (11)$$

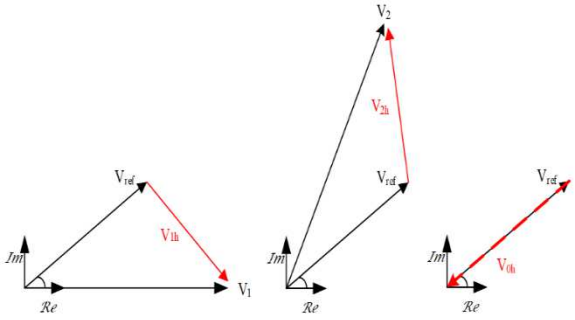

Fig 4. Vector diagram of the first sector of the inverter hexagon.

The modulation index and reference vector position define the magnitude and phase of each harmonic voltage vector. In addition, the duty cycles of the adjacent active vectors (d_1 and d_2) and the two zero vectors distribution (d_0 and d_7) determine the trajectories of the harmonic currents[26].

Hence, the harmonic flux φ_h in the N'th carrier cycle is defined as the time integral of the harmonic voltage vector V_{kh} as defined in (12).

$$\varphi_h = \int_{NT_s}^{(N+1)T_s} (V_k - V_{ref}) dt \quad (12)$$

V_k is the inverter output voltage vector of the k'th state in the carrier cycle that changes according to the selected switching sequence.

In most applications, the inductive effect is dominant over the resistive effect for high switching frequencies (f_s/f_e> 20)[25]. So, the harmonic current and harmonic flux trajectories have the same trajectories at a scale factor ($\varphi = Li$).

For example, in the first sector of the inverter's hexagon, the vector sequence: V_7- V_2- V_1- V_0- V_0- V_1- V_2- V_7 is generated, and hence a particular trajectory of the harmonic flux is defined according to the above closed integral (equation 12). During the sampling time, this trajectory is unchangeable due to the high ratio between the sampling frequency f_s and the reference voltage frequency f as well as the constant values of the reference voltage vector V_{ref} and the output voltage vector V_k.

The value of the harmonic flux is calculated by using equation (12) and the predefined above sequence. It is noticed that this value becomes null at the beginning (V_7), the half (V_0) at the end (V_7) of the sequence.

Since the SVPWM sequence is symmetrical, it is sufficient to calculate the harmonic flux only for the first half of the sequence and hence it is systematically computed for the second one. Therefore, the obtained flux trajectories describe two symmetrical triangles regarding the line of the reference vector (Fig 5). The displacement and the shape of the triangles, which directly represent the harmonic content, depend respectively on the reference vector position and the ZVD. Since the reference vector position is imposed directly by the load, the harmonic content can be affected only by changing the ZVD. So, the proposed SVPWM technique is based on computing the optimal ZVD to improve as possible the harmonic content.

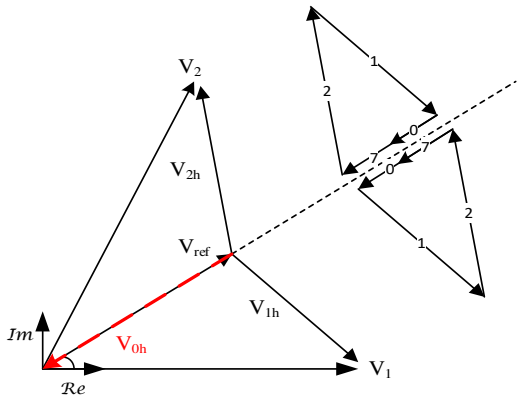

Fig 5. Harmonic flux trajectories in the first sector of the inverter hexagon.

II.3. *Mathematical development of the harmonic flux*

In order to detail the proposed optimized ZVD, it is necessary to calculate the flux harmonic for each sector of the hexagon. For sector 1, the output voltage vector V_k can take the different values given in equation (13) according to the half sequence.

$$\vec{V_k} = \begin{cases} \vec{V}_7 = \vec{0} \\ \vec{V}_1 = \frac{2}{3}V_{dc} \\ \vec{V}_2 = \frac{2}{3}V_{dc}e^{j\frac{\pi}{3}} \\ \vec{V}_0 = \vec{0} \end{cases} \tag{13}$$

By replacing V_k with its values given above in equation (12), the harmonic flux for the half sequence can be expressed as follows:

$$\varphi_{h1} = \begin{cases} -V_{ref}e^{j\theta}d & 0 \le d \le d_7 \\ -\frac{2V_{dc}}{3}e^{j\frac{\pi}{3}}d_7 + \left(\frac{2V_{dc}}{3}e^{j\frac{\pi}{3}} - V_{ref}e^{j\theta}\right)d & d_7 \le d \le d_7 + d_2 \\ -V_{ref}e^{j\theta}\left(d_7 + d_2\right) + \frac{2V_{dc}}{3}e^{j\frac{\pi}{3}}d_2 & \\ +\left(\frac{2V_{dc}}{3} - V_{ref}e^{j\theta}\right)\left(d - d_7 - d_2\right) & d_7 + d_2 \le d \le d_7 + d_2 + d_1 \\ \frac{2V_{dc}}{3}\left(d_1 + d_2e^{j\frac{\pi}{3}}\right) - V_{ref}e^{j\theta}d & d_7 + d_2 + d_1 \le d \le 1 \end{cases} \tag{14}$$

d is the variable duty cycle of the inverter state during a half sequence, and varies between 0 and 1.

To express the flux harmonic φ_{h1} as a function of the modulation index m, the reference vector position θ and ZVD d_7, the equations (15) and (16) have been used to obtain the equation (17) as shown below:

$$\varphi_1 = \frac{\varphi_{h1}}{\varphi_b} \tag{15}$$

$$\varphi_b = \frac{2V_{dc}}{\pi} \tag{16}$$

$$\varphi_1 = \begin{cases} -me^{j\theta}d & 0 \le d \le d_7 \\ -\frac{\pi}{3}e^{j\frac{\pi}{3}}d_7 + \left(\frac{\pi}{3}e^{j\frac{\pi}{3}} - me^{j\theta}\right)d & d_7 \le d \le d_7 + d_2 \\ me^{j\theta}\left(d_7 + d_2\right) + \frac{\pi}{3}e^{j\frac{\pi}{3}}d_2 & \\ +\left(\frac{\pi}{3} - me^{j\theta}\right)\left(d - d_7 - d_2\right) & d_7 + d_2 \le d \le d_7 + d_2 + d_1 \\ \frac{\pi}{3}\left(d_1 + d_2e^{j\frac{\pi}{3}}\right) - me^{j\theta}d & d_7 + d_2 + d_1 \le d \le 1 \end{cases} \tag{17}$$

The flux harmonic of the second sequence half is symmetrical to the first one, hence it is simply determined with the symmetry condition mentioned in the following equation.

$$\varphi_2(d) = \varphi_1(1-d) \tag{18}$$

Therefore, the generalized expression of the harmonic flux of each sector of the inverter hexagon can be deduced as follows:

$$\varphi_1 = \begin{cases} -me^{j\theta}d & 0 \le d \le d_7 \\ -\frac{\pi}{3}e^{j\frac{s\pi}{3}}d_7 + \left(\frac{\pi}{3}e^{j\frac{s\pi}{3}} - me^{j\theta}\right)d & d_7 \le d \le d_7 + d_{s+1} \\ me^{j\theta}\left(d_7 + d_{s+1}\right) + \frac{\pi}{3}e^{j\frac{s\pi}{3}}d_{s+1} & \\ +\left(\frac{\pi}{3} - me^{j\theta}\right)\left(d - d_7 - d_{s+1}\right) & d_7 + d_{s+1} \le d \le d_7 + d_{s+1} + d_s \\ \frac{\pi}{3}\left(d_s + d_{s+1}e^{j\frac{s\pi}{3}}\right) - me^{j\theta}d & d_7 + d_{s+1} + d_s \le d \le 1 \end{cases} \quad (19)$$

$$\varphi_{2s}(d) = -\varphi_{1s}(1-d) \quad (20)$$

It is clearly shown in Fig 5 that the harmonic flux trajectories, drawn by using equation (20), depend mainly on the modulation index *m* (Fig 6.(a)), angle θ (Fig 6.(b)) and ZVD (Fig 6.(c)).

It can be seen from Fig 6.(a) that the triangle surface decreases when the modulation index increases. This result confirms that the harmonic flux and consequently the harmonic content are inversely proportional to the modulation index. Likewise, the triangle's shape varies with the variation of angle θ with the same modulation index m = 0.7 (Fig 6.(b)). So, the harmonic flux and consequently the harmonic content change with the voltage reference position. Similarly, it is obvious from Fig 6.(c) that the triangles slide with change in ZVD and hence their gravity center displace. It is clearly noticed also that the gravity center of the dashed triangle is the closest one to the origin *O* and consequently it can be said that $d_7 = 0.5d_z$ is the best value of ZVD for lower generated harmonic content since the distance to the origin is equal the magnitude of the harmonic flux [25]. Therefore, it is appropriate to determine the optimal ZVD which gives the closest gravity center to the origin, and this is for any modulation index m and any angle θ.

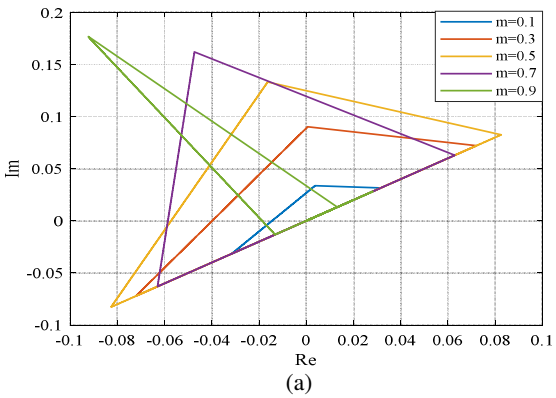

(a)

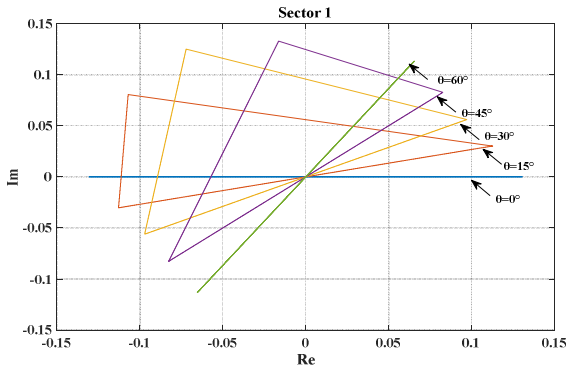

(b)

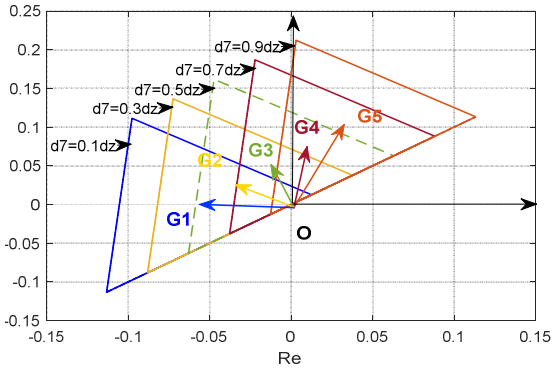

(c)

Fig 6. Different trajectories of the harmonic flux. (a) Different modulation index CSVPWM. (b) Different angles m=0.7 with CSVPWM. (c)Different ZVD m=0.7 and θ=45°.

II.4. Mathematical Development Of The Optimized ZVD

This subsection is dedicated to compute the optimal ZVD to allow a lower harmonic content generation, thus the closest gravity center of the triangle, representing the harmonic flux trajectory, to the origin *O*. For the symmetry reason, the sector 1 and the first half sequence are taken as an instance. As the harmonic flux trajectory is a triangle, which i defined by three summits (a_1, a_2, and a_3) and gravity center *G*. since the summits are the extremities of the triangle trajectory, defined by equation (17), their expression is given as follows:

$$\begin{cases} \overrightarrow{oa_1} = -me^{j\theta}d_7 \\ \overrightarrow{oa_2} = \left(\frac{\pi}{3}e^{j\frac{\pi}{3}} - me^{j\theta}\right)d_2 - me^{j\theta}d_7 \\ \overrightarrow{oa_3} = \frac{\pi}{3}(d_1 + e^{j\frac{\pi}{3}}d_2) - me^{j\theta}(d_7 + d_2 + d_1) \end{cases} \quad (21)$$

The gravity center vector $\overrightarrow{OG}$ of a triangle with summits (a_1, a_2, and a_3) is expressed as follows:

$$\overrightarrow{OG} = \frac{1}{3}\left(\overrightarrow{oa_1} + \overrightarrow{oa_2} + \overrightarrow{oa_3}\right) \quad (22)$$

By replacing (21) in (22), the gravity center vector $\overrightarrow{OG}$ can be expressed as a function of ZVD (d_7), as follows:

$$\overrightarrow{OG}=\frac{1}{3}\left(-me^{j\theta}\left(3d_7+2d_2+d_1\right)+\left(\frac{2\pi}{3}e^{j\frac{\pi}{3}}d_2+\frac{\pi}{3}d_1\right)\right)$$

(23)

The module of the gravity center vector $\left\|\overrightarrow{OG}\right\|$, which reflects the magnitude of the harmonic flux, is given by:

$$\left\|\overrightarrow{OG}\right\|=\frac{1}{3}\sqrt{\begin{array}{l}\left(\left(-m\cos\theta\left(3d_7+2d_2+d_1\right)+\left(\frac{2\pi}{3}\cos\left(\frac{\pi}{3}\right)d_2+\frac{\pi}{3}d_1\right)\right)^2+\\ \left(-m\sin\theta\left(3d_7+2d_2+d_1\right)+\left(\frac{2\pi}{3}\sin\left(\frac{\pi}{3}\right)d_2\right)\right)^2\end{array}}$$

(24)

The optimum of ZVD (d_7) that ensures the minimum of the module $\left\|\overrightarrow{OG}\right\|$ can be found by resolving the equation (24)

$$\frac{\partial\left\|\overrightarrow{OG}\right\|}{\partial d_7}=\frac{1}{6}\frac{\left(\begin{array}{l}\left(\left(-m\cos\theta\left(3d_7+2d_2+d_1\right)+\left(\frac{2\pi}{3}\cos\left(\frac{\pi}{3}\right)d_2+\frac{\pi}{3}d_1\right)\right)^2+\\ \left(-m\sin\theta\left(3d_7+2d_2+d_1\right)+\left(\frac{2\pi}{3}\sin\left(\frac{\pi}{3}\right)d_2\right)\right)^2\end{array}\right)'}{\left\|\overrightarrow{OG}\right\|}$$

(25)

Then optimum d_7 is obtained as:

$$d_7=\frac{1}{3m}\left(\frac{2\pi}{3}d_2\left(\cos\left(\theta-\frac{\pi}{3}\right)\right)+\frac{\pi}{3}d_1\cos\theta\right)-\frac{2}{3}d_2-\frac{1}{3}d_1$$

(26)

The general expression of the ZVD for each sector (s) in the hexagon is obtained as follows:

$$\begin{cases}d_7=\frac{1}{3m}\left(\frac{2\pi}{3}d_{s+1}\left(\cos\left(\theta-\frac{\pi}{3}\right)\right)+\frac{\pi}{3}d_s\cos\theta\right)-\frac{2}{3}d_{s+1}-\frac{1}{3}d_s\\ d_0=d_z-d_7\end{cases}$$

(27)

II.5. *Graphical Presentation Of The Gravity Center Vector*

The displacement of the gravity center depends on the variation of the zero vector distribution as shown in Fig 7.(a), which is a 3-D representation of this displacement according to the angle θ and the ZVD for m=0.2, it is obvious that it exists an optimal ZVD which ensures a minimum distance of the gravity center to the origin which drawn in red on Fig 7. (a). This optimal distance is obtained from equation (27). To make it simpler, Fig 7. (b) is the longitudinal section of Fig 7.(a), where the displacement of the gravity center versus the angle θ is presented for different ZVD.

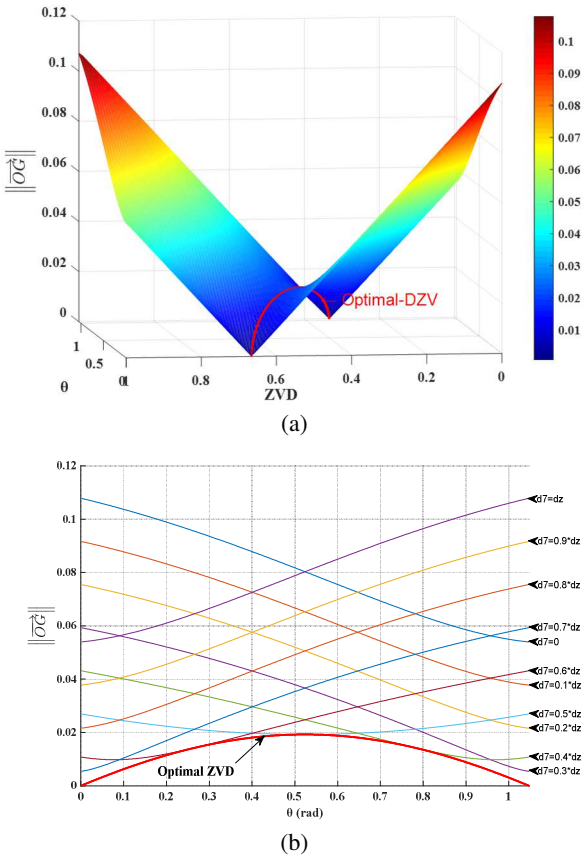

Fig 7. Center gravity displacement. (a) 3-D displacement presentation. (b) Longitudinal section displacement.

In order to illustrate the harmonic content improvement, a 3-D graphical presentation of the gravity center vector enables the comparison with CSVPWM and R-ZVD-SVPWM. Fig 8 represents the displacement of the gravity center vector versus the modulation index m and the angle θ. It can be seen that the curve presenting the gravity center vector obtained by using the proposed technique is situated below the one issued by using the CSVPWM (Fig 8.(a)). Similarly, the same result is illustrated in Fig 8.(b) when the proposed technique is compared with R-ZVD-SVPWM. Therefore, the module of the gravity center vector and hence the equivalent harmonic content is less when using the proposed technique thanks to the use of the optimal calculated ZVD defined by equation (27).

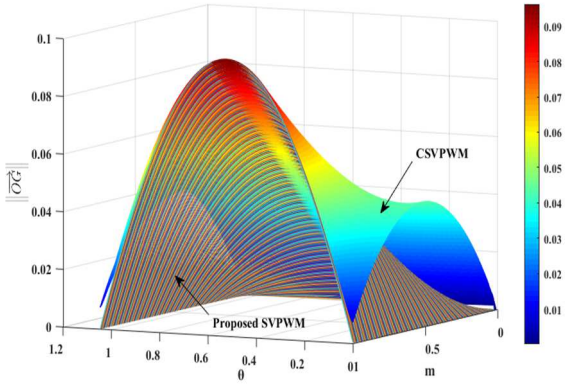

(a)

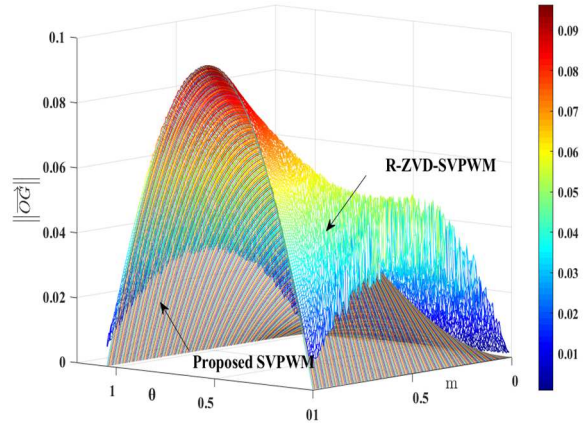

(b)

Fig 8. 3-D graphical presentation of the gravity center displacement. (a) CSVPWM and the proposed SVPWM. (b) R-ZVD-SVPWM and the proposed SVPWM.

III. SIMULATION RESULTS

This section presents the simulation results (under MATLAB/Simulink) of the CSVPWM, R-ZVD-SVPWM ,and the proposed technique applied to a three-phase VSI supplying a three-phase load (R=1.6Ω, L=4mH) with a switching frequency f_s=10 kHz and V_{DC}=200V.

Fig 9 shows the phase reference voltage of each modulation technique for different modulation indexes. It is clearly seen from Fig 9.(a) that the magnitude of the reference voltage for the CSVPWM increases with the modulation index, whereas its shape remains unchanged. Similarly, it is shown for the R-ZVD-SVPWM that the reference voltage (Fig 9.(b)) has almost the same shape as the CSVPWM with a thick line due to the effect of the zero vectors random distribution but this effect decreases with the increasing of the modulation index. However, it is observed for the proposed SVPWM that the reference voltage (Fig 9.(c)) for each modulation index has its specific shape.

Fig 10 shows the shape of the line current which is improved with the increasing of the modulation index for the three modulation techniques. However, for low modulation index such as for *m*=0.1 or *m*=0.2, the obtained current with the CSVPWM (Fig 10.(a)) has not a sinusoidal shape and consequently it has a high harmonic content.

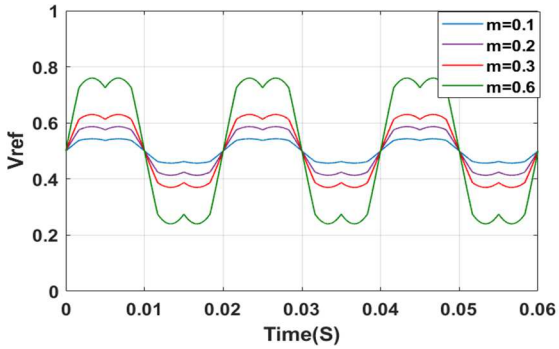

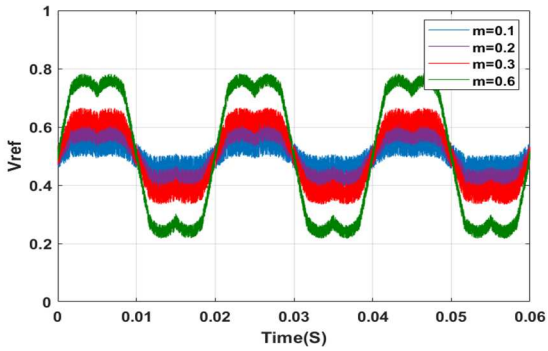

(b)

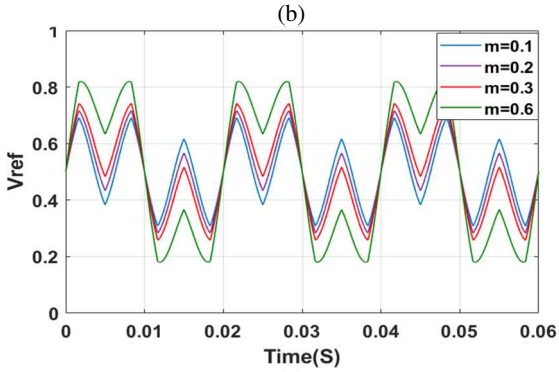

(c)

Fig 9. Phase voltage reference. (a) CVPWM. (b) R-ZVD-SVPWM. (c) Proposed SVPWM.

The R-ZVD-SVPWM improves slightly the shape of the current at modulation indexes greater than 0.2 (Fig 10.(b)), but the magnitude of the current is not stable. Unlike the two mentioned modulation techniques the current generated by the proposed SVPWM (Fig 10.(c)) has a sinusoidal shape with low harmonic content and stable magnitude.

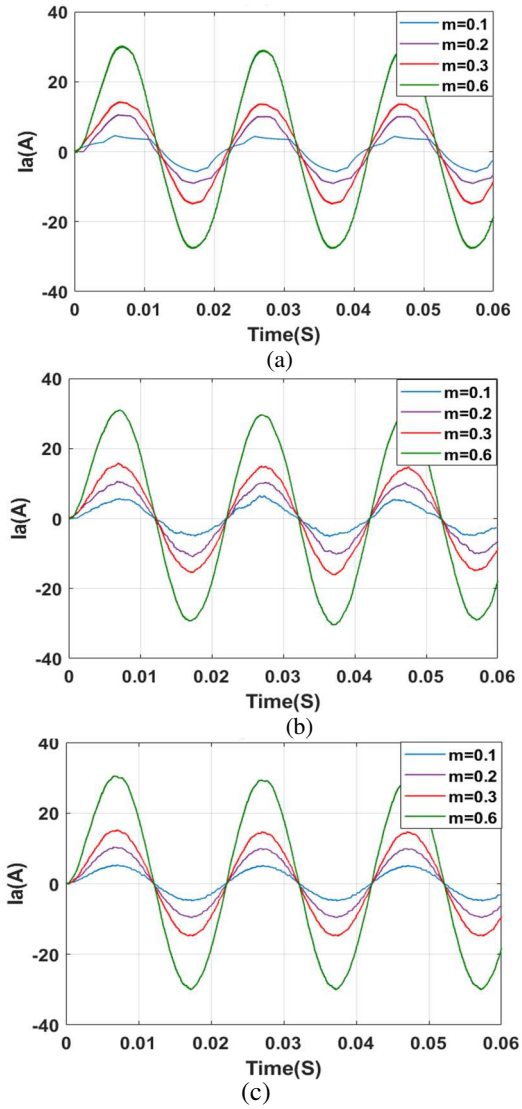

Fig 10. Line courant output. (a) CVPWM. (b) R-ZVD-SVPWM.(c) Proposed SVPWM.

Fig 11.(a), 11.(b) and 11.(c) illustrate respectively the line current trajectory in α-β reference frame of the three modulation techniques: CSVPWM, R-ZVD-SVPWM and proposed SVPWM. It is obviously shown that the line current trajectory of the CSVPWM (Fig 11.(a)) has a hexagonal shape for low modulation indexes and becomes circular with high modulation indexes. Moreover, the line current trajectory of the R-ZVD-SVPWM (Fig 11.(b)) has an overlapping circles shape for low modulation indexes due to the random distribution of the zero vectors and this shape will be enhanced with the increasing of the modulation indexes. However, the line current trajectory of the proposed SVPWM (Fig 11.(c)) has a circular current trajectory for the whole modulation index range.

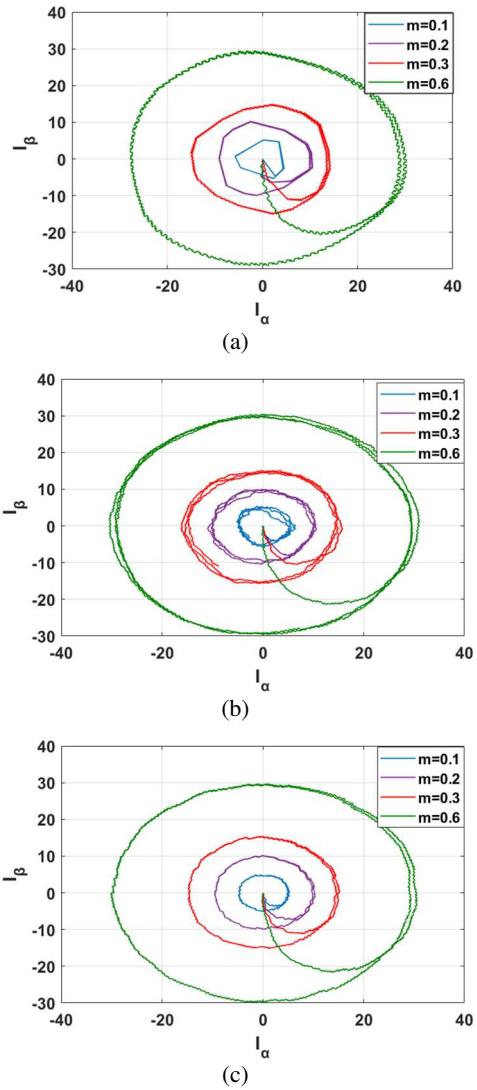

Fig 11. Line current trajectories in α-β plan reference frame.(a) CVPWM. (b) R-ZVD-SVPWM. (c) Proposed SVPWM.

Fig 12 illustrates the spectral analysis of the three modulation techniques. It is clearly noticed that the proposed SVPWM has the lowest harmonic content compared to the CSVPWM and R-ZVD-SVPWM especially for low modulation index (Fig 12.(a) and Fig 12.(b)). Likewise, it is obviously observed also that the obtained spectra of the proposed SVPWM still lower than the two other modulation techniques for the different modulation index.

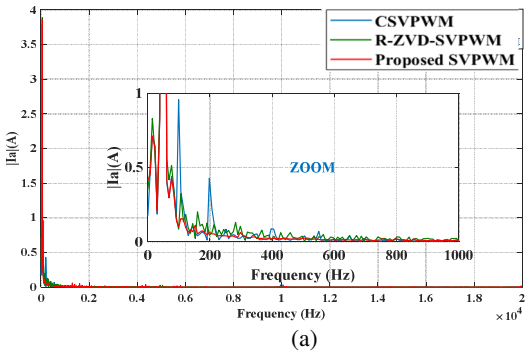

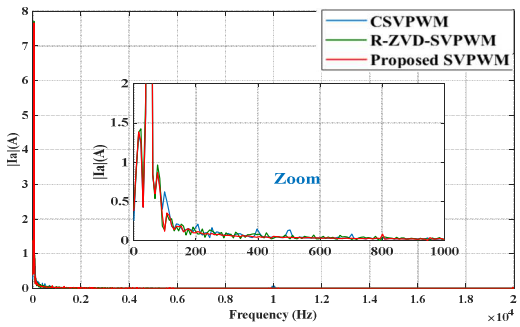

(b)

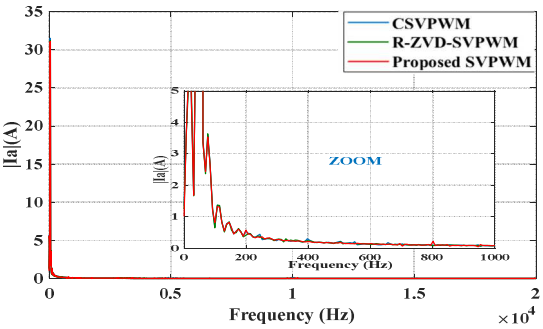

(c)

Fig 12. Spectral analysis for line current. (a) m=0.1.(b) m=0.2.(c)m=0.6.

IV. EXPERIMENTAL RESULTS

The experimental test bench is composed of a three-phase R-L load (R=1.6Ω, L=4mH) fed by a VSI. The proposed SVPWM, CSPWM and R-ZVD-SVPWM are implemented on a dSPACE DS1104 board, as shown in Fig 13. The switching frequency is set to f_s=10 kHz and V_{DC}=200V.

Fig 13. Photography of the experimental test bench.

The obtained experimental results are totally agreed with the simulation results. For example, Fig 14 to Fig 17 illustrate the measured line current for different modulation indexes m=0.1 (Fig 14), m=0.3 (Fig 15), and m =0.6 (Fig 16). Firstly, it can be observed that the shape of the waveforms is improved when the modulation index increases. However, the proposed SVPWM exhibits the best performances with a sinusoidal current waveform for all the modulation indexes unlike the conventional SVPWM and the random R-ZVD-SVPWM.

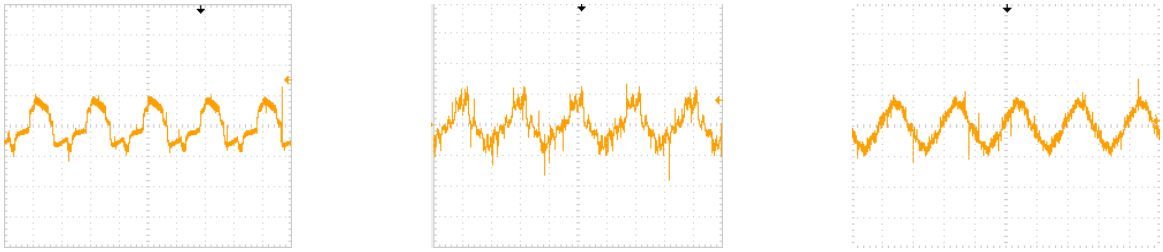

(a) (b) (c)

Fig 14. Measured line current output with *m* =0.1(5A/div., 10ms/div.).(a) CSVPWM. (b) R-ZVD-SVPWM. (c) Proposed SVPWM

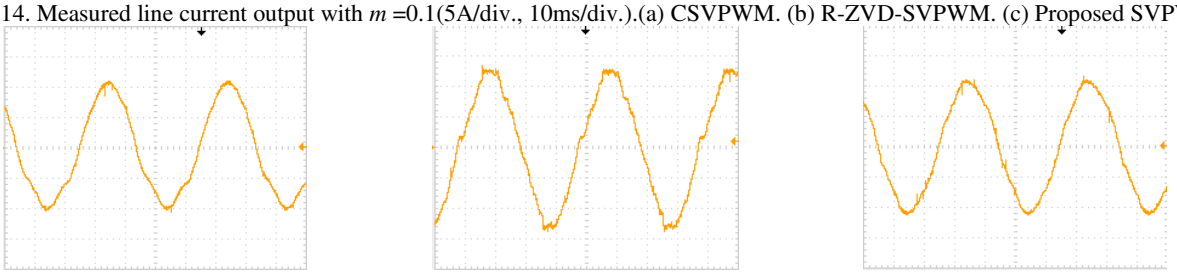

(a) (b) (c)

Fig 15. Measured line current output with *m* =0.3(10A/div., 5ms/div.).(a) CSVPWM. (b) R-ZVD-SVPWM. (c) Proposed SVPWM.

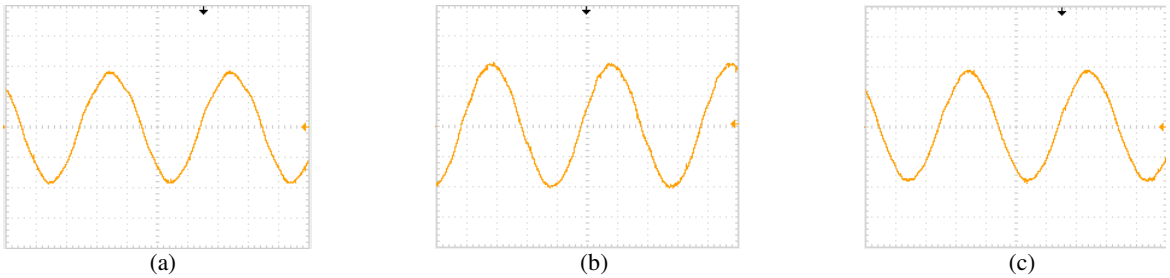

(a) (b) (c)

Fig 16. Measured line current output with *m* =0.6(20A/div., 5ms/div.).(a) CSVPWM. (b) R-ZVD-SVPWM. (c) Proposed SVPWM.

Fig 17 to 19 show the line current trajectories in α-β reference frame for different modulation indexes: *m*=0.1 (Fig 16), *m*=0.3 (Fig 17) and *m* =0.6 (Fig 18). Likewise, the trajectories are circular at high modulation index for the three modulation techniques. However, only for the proposed technique the line current presents a circular trajectory at low modulation indexes.

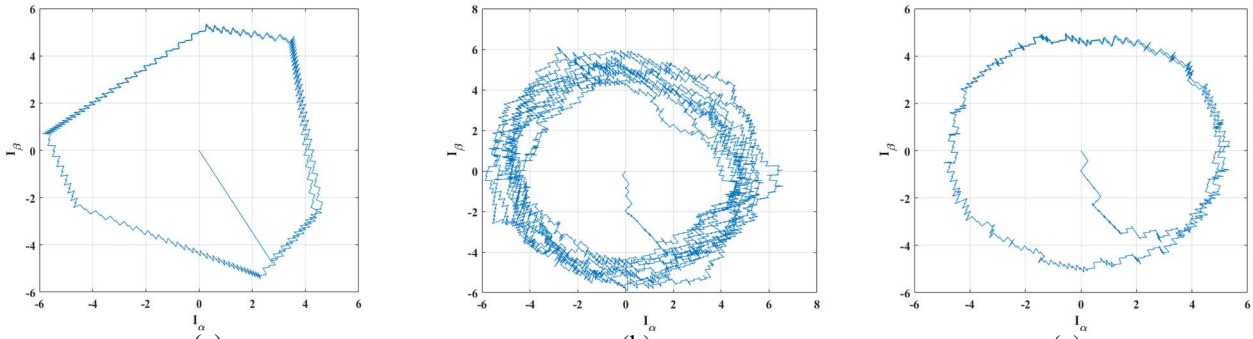

(a) (b) (c)

Fig 17. Line current trajectories in α-β reference frame with *m*=0.1(a) CSVPWM. (b) R-ZVD-SVPWM. (c) Proposed SVPWM.

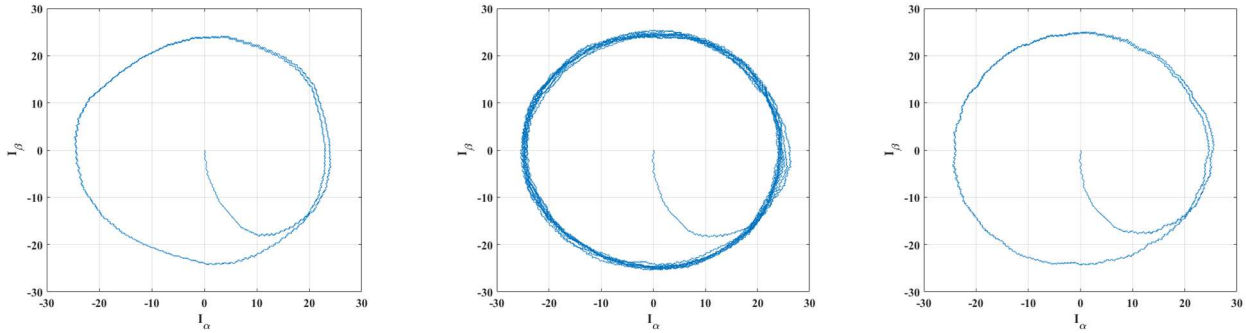

(a) (b) (c)

Fig 18**.** Line current trajectories in α-β reference frame with *m* =0.3(a) CSVPWM. (b) R-ZVD-SVPWM. (c) Proposed SVPWM.

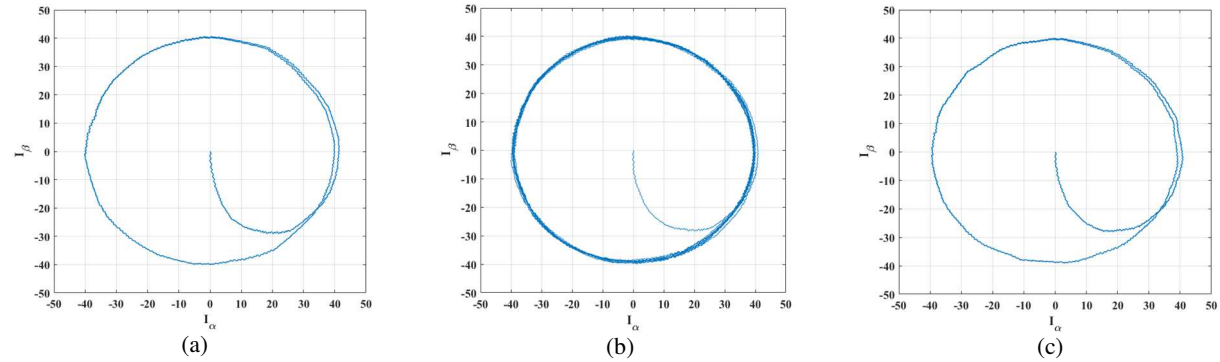

(a) (b) (c)

Fig 19. Line current trajectories in α-β reference frame with *m* =0.6.(a) CSVPWM. (b) R-ZVD-SVPWM. (c) Proposed SVPWM.

Fig 20 illustrates the measured line current THD of the three modulation techniques for the complete modulation index range and presents good performances when the modulation index is low, for example when m=0.1 the index range. This Fig confirms clearly that the proposed technique has the lowest THD for the whole modulation THD are respectively equal to 35.8% (CSVPWM), 24%(R-ZVD-SVPWM), and16,9% (Proposed SVPWM).

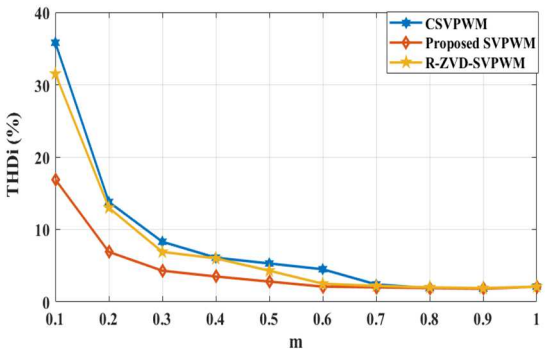

Fig 20. Measured phase current output THD.

V. CONCLUSION

In today's industry, controlled VSI is considered a fundamental means to control electrical systems either for power conversion or for power drive, where energy quality and efficiency have to be taken into consideration. This paper has proposed a new SVPWM scheme, based on an optimized distribution of the zero vectors, for the purpose of enhancing the system efficiency. This strategy has used an analytical development of the flux harmonic aspect, which permits an exact mathematical formulation of the zero vector duration and hence an optimized ZVD. This technique has provided a gain in fundamental current and voltage outputs that upgraded imperatively the system efficiency. In addition, the voltage and current waveforms are improved and therefore the total harmonic distortion is improved particularly for low modulation index. The validity of the proposed technique has been verified through simulation by using Simulink/MATLAB and proved by an experimental test bench. Both simulation and experimental results have shown good performances of the proposed SVPWM technique compared to the CSVPWM and R-ZVD-SVPWM, especially for low modulation index. Besides the yield gain that offers this technique, its ease of implementation on a modern processor makes it favorable to be simply industrialized.

REFERENCES

[1] T. Ghennam, E. M. Berkouk, and B. Francois, A Novel Space-Vector Current Control Based on Circular Hysteresis Areas of a Three-Phase Neutral-Point-Clamped Inverter,l*IEEE Transactions on Industrial Electronics*, *vol. 57, no. 8, pp. 2669–2678*, Aug. 2010, doi: 10.1109/TIE.2009.2035458.

[2] K. Marouani, L. Baghli, D. Hadiouche, A. Kheloui, and A. Rezzoug, A New PWM Strategy Based on a 24-Sector Vector Space Decomposition for a Six-Phase VSI-Fed Dual Stator Induction Motor, *IEEE Transactions on Industrial Electronics, vol. 55, no. 5, pp. 1910–1920*, May 2008, doi: 10.1109/TIE.2008.918486.

[3] A. Verma, R. Krishan, and S. Mishra, A Novel PV Inverter Control for Maximization of Wind Power Penetration, *IEEE Transactions on Industry Applications, vol. 54, no. 6, pp. 6364–6373*, Nov. 2018, doi: 10.1109/TIA.2018.2854875.

[4] V. Lakshmi Srinivas, B. Singh, S. Mishra, and L. Xu, Harmonic Voltage Control in Distributed Generation Systems Using Optimal Switching Vector Strategy, *IEEE Systems Journal, vol. 16, no. 2, pp. 1861–1872*, Jun. 2022, doi: 10.1109/JSYST.2021.3070498.

[5] C. Zhang, J. M. Guerrero, J. C. Vasquez, and E. A. A. Coelho, Control Architecture for Parallel-Connected Inverters in Uninterruptible Power Systems, *IEEE Transactions on Power Electronics, vol. 31, no. 7, pp. 5176–5188,* Jul. 2016, doi: 10.1109/TPEL.2015.2481480.

[6] L. Asiminoaei, P. Rodriguez, F. Blaabjerg, and M. Malinowski, Reduction of Switching Losses in Active Power Filters With a New Generalized Discontinuous-PWM Strategy, *IEEE Transactions on Industrial Electronics, vol. 55, no. 1, pp. 467–471*, Jan. 2008, doi: 10.1109/TIE.2007.896554.

[7] V. L. Srinivas, B. Singh, and S. Mishra, Enhanced Power Quality PV Inverter With Leakage Current Suppression for Three-Phase SECS, *IEEE Transactions on Industrial Electronics, vol. 69, no. 6, pp. 5756–5767*, Jun. 2022, doi: 10.1109/TIE.2021.3090698.

[8] Anas Ibrahim, Muhamad Zahim Sujod, Variable switching frequency hybrid PWM technique for switching loss reduction in a three-phase two-level voltage source inverter, *Measurement, vol. 151, p. 107192*, Feb. 2020, doi: 10.1016/j.measurement.2019.107192.

[9] Y. Tang, Y. He, F. Wang, and R. Kennel, Voltage-Sourced Converter Fed High-Speed Switched Reluctance Motor Drive System With Energy Feedback and Near-Unity Power Factor, *IEEE Transactions on Industrial Electronics, vol. 69, no. 4, pp. 3460–3470*, Apr. 2022, doi: 10.1109/TIE.2021.3073304.

[10] M. Stender, O. Wallscheid, and J. Böcker, Accurate Torque Control for Induction Motors by Utilizing a Globally Optimized Flux Observer, *IEEE Transactions on Power Electronics, vol. 36, no. 11, pp. 13261–13274*, Nov. 2021, doi: 10.1109/TPEL.2021.3080129.

[11] F. Z. Peng, M. Shen, and K. Holland, Application of Z-Source Inverter for Traction Drive of Fuel Cell—Battery Hybrid Electric Vehicles, *IEEE Transactions on Power Electronics, vol. 22, no. 3, pp. 1054–1061*, May 2007, doi: 10.1109/TPEL.2007.897123.

[12] Y. Liu, K. Y. See, R. Simanjorang, A. Nawawi, and L. Ziyou, Harmonics and common mode voltage analysis with different power converter conFigurations in aerospace applications, *Asia-Pacific International Symposium on Electromagnetic Compatibility (APEMC),* Jun. 2017, pp. 82–84. doi: 10.1109/APEMC.2017.7975431.

[13] K. Nounou, J. F. Charpentier, K. Marouani, M. Benbouzid, and A. Kheloui, Emulation of an Electric Naval Propulsion System Based on a Multiphase Machine Under Healthy and Faulty Operating Conditions, *IEEE Transactions on Vehicular Technology, vol. 67, no. 8, pp. 6895–6905,* Aug. 2018, doi: 10.1109/TVT.2018.2834342.

[14] J. Wei, X. Kong, W. Tao, Z. Zhang, and B. Zhou, The Torque Ripple Optimization of Open-Winding Permanent Magnet Synchronous Motor With Direct Torque Control Strategy Over a Wide Bus Voltage Ratio Range, *IEEE Transactions on Power Electronics, vol. 37, no. 6, pp. 7156–7168*, Jun. 2022, doi: 10.1109/TPEL.2022.3146155.

[15] Y. Huang, Y. Xu, W. Zhang, and J. Zou, Hybrid RPWM Technique Based on Modified SVPWM to Reduce the PWM Acoustic Noise, *IEEE Transactions on Power Electronics, vol. 34, no. 6, pp. 5667–5674,* Jun. 2019, doi: 10.1109/TPEL.2018.2869980.

[16] Y. Lian, Y. W. Li, Z. Quan, N. R. Zargari, and Z. Cheng, SVM Strategies for Common-Mode Current Reduction in Transformerless Current-Source Drives at Low Modulation Index, *IEEE Transactions on Power Electronics, vol. 32, no. 2, pp. 1312–1323*, Feb. 2017, doi: 10.1109/TPEL.2016.2544785.

[17] D. Wu and L. Peng, Analysis and Suppressing Method for the Output Voltage Harmonics of Modular Multilevel Converter, *IEEE Transactions on Power Electronics, vol. 31, no. 7, pp. 4755–4765*, Jul. 2016, doi: 10.1109/TPEL.2015.2482496.

[18] W. Jiang, Q. Wang, Q. Chen, and C. Hu, A simplified SVPWM control algorithm for multilevel VSI based two-level SVPWM control algorithm, *International Conference on Electrical Machines and Systems (ICEMS)*, Oct. 2007, pp. 43–49. doi: 10.1109/ICEMS12746.2007.4412137.

Manuscript received January 2013, revised February 2013

[19] J. Zhou, Y. Yuan, and H. Dong, Adaptive DC-Link Voltage Control for Shunt Active Power Filters Based on Model Predictive Control, *IEEE Access, vol. 8, pp. 208348–208357*, 2020, doi: 10.1109/ACCESS.2020.3038459.

[20] J. Lee, M.-W. Kim, I. Kim, and J.-W. Park, Analysis of DC-Link Voltage Ripple by Generalized Discontinuous PWM Strategy in Two-Level Three-Phase Voltage Source Inverters, *IEEE Transportation Electrification Conference & Expo (ITEC),* Jun. 2022, pp. 49–54. doi: 10.1109/ITEC53557.2022.9814042.

[21] D. G. Holmes and T. A. Lipo, Pulse Width Modulation for Power Converters: Principles and Practice. John Wiley & Sons, 2003.

[22] Y.-C. Lim, Y.-G. Jung, S.-Y. Oh, and J.-G. Kim, A Two-Phase Separately Randomized Pulse Position PWM (SRP-PWM) Scheme With Low Switching Noise Characteristics Over the Entire Modulation Index, *IEEE Transactions on Power Electronics, vol. 27, no. 1, pp. 362–369,* Jan. 2012, doi: 10.1109/TPEL.2010.2087361.

[23] R. Gamoudi, D. Elhak Chariag, and L. Sbita, A Review of Spread-Spectrum-Based PWM Techniques—A Novel Fast Digital Implementation, *IEEE Transactions on Power Electronics, vol. 33, no. 12, pp. 10292–10307*, Dec. 2018, doi: 10.1109/TPEL.2018.2808038.

[24] A. Boudouda, N. Boudjerda, K. El Khamlichi Drissi, and K. Kerroum, Combined random space vector modulation for a variable speed drive using induction motor, *Electr Eng, vol. 98, no. 1, pp. 1–15*, Mar. 2016, doi: 10.1007/s00202-015-0341-6.

[25] A. M. Hava, R. J. Kerkman, and T. A. Lipo, Simple analytical and graphical methods for carrier-based PWM-VSI drives, *IEEE Transactions on Power Electronics, vol. 14, no. 1, pp. 49–61,* Jan. 1999, doi: 10.1109/63.737592.

[26] A. M. Hava and N. O. Çetin, A Generalized Scalar PWM Approach With Easy Implementation Features for Three-Phase, Three-Wire Voltage-Source Inverters, *IEEE Transactions on Power Electronics, vol. 26, no. 5, pp. 1385–1395,* May 2011, doi: 10.1109/TPEL.2010.2081689.

Authors' information

Hichem BENKADI was born in Algiers, Algeria in 1988. He received the Engineering and master's degrees in 2011 and 2017 respectively in Electrical Engineering from the Ecole Militaire Polytechnique of Algiers, Algeria (EMP). Currently, he is a PhD student- in electrical engineering at EMP. His main research interests include power electronics, power drives and power systems. And embedded power systems.

Tarak Ghennam was born in Ain Kercha, Oum El-Bouaghi, Algeria in 1977. He received the Engineering, master's and PHD degrees in 2000, 2005 and 2011 respectively in Electrical Engineering from the Ecole Militaire Polytechnique of Algiers, Algeria (EMP). In 2016, he obtained the 'Habilité à Diriger des Recherches (HDR)' degree. Currently he is a Teacher-Researcher in electrical engineering at EMP. His main research interests include power electronics, power drives and renewable energy based power systems.

Khoudir Marouani received the Engineer, Magister and Ph.D. degrees in electrical engineering from the Ecole Militaire Polytechnique (EMP), Algiers, Algeria, in 1996, 2000 and 2010, respectively. He obtained the Habilitation Universitaire degree in 2017.

He is currently a Teacher-Researcher in electrical engineering at EMP and Université Mouloud Mammeri de Tizi-Ouzou (UMMTO). He authored or co-authored more than 50 technical papers in refereed journals and conference proceedings. His research interests include power electronics, electrical drives and Hybrid Electric Vehicles (HEV).

Nassim Rizoug received the Engineering degree from the E.N.P. (Ecole Polytechnique d'Alger), Algiers, Algeria, in 1998, and the Ph.D. degree in electrical engineering from the Ecole Centrale de Lille, France, in 2006.,Since 2007, he has been an Assistant Professor with the Ecole Supérieure des Techniques Aéronautiques et de Construction Automobile (ESTACA), Laval, France. His research interests include the field of energy management and the characterization of the storage component for the power electronic applications.

Mohamed Benbouzid received the Ph.D. degree in electrical and computer engineering from the National Polytechnic Institute of Grenoble, Grenoble, France, in 1994, and the Habilitation à Diriger des Recherches degree from the University of Amiens, Amiens, France, in 2000.,After receiving the Ph.D. degree, he joined the University of Amiens, where he was an Associate Professor of electrical and computer engineering. Since September 2004, he has been with the University of Brest, Brest, France, where he is currently a Full Professor of electrical engineering. He is also a Distinguished Professor and a 1000 Talent Expert at Shanghai Maritime University, Shanghai, China. His main research interests and experience include the analysis, design, and control of electric machines; variable-speed drives for traction, propulsion, and renewable energy applications; and fault diagnosis of electric machines.,Dr. Benbouzid is a fellow of the IET. He is the Editor-in-Chief of the International Journal on Energy Conversion and the Applied Sciences (MDPI) Section on Electrical, Electronics and Communications Engineering. He is a Subject Editor of the IET Renewable Power Generation.

Bruno Francois received the Ph.D. degree in electrical engineering from the University of Lille, Lille, France, in 1996. In 1996, he joined the Department of Electrical Engineering, Centrale Lille, Villeneuve-d'Ascq, France, as an Associate Professor and then as a Full Professor in 2011. He is currently a Researcher with the Laboratory of Electrical Engineering and Power electronics (L2EP), Lille, France. He is currently working on the advanced energy management systems for power systems, architectures and control systems of future electrical networks, and uncertainty impacts in operation of electrical systems.

